ACS Sustainable Chemistry & Engineering

Research Article

pubs.acs.org/journal/ascecg

Method To Characterize Acid–Base Behavior of Biochar: Site Modeling and Theoretical Simulation

Mi Li,[†] Qiang Liu,*[,†] Zhenjun Lou,[†] Yang Wang,[†] Yaping Zhang,[‡] and Guangren Qian*[,†]

[†]School of Environmental and Chemical Engineering, Shanghai University, No. 99 Shangda Road, Shanghai 200444, China

[‡]Engineering Research Center of Biomass Materials (SWUST), Ministry of Education, No. 59 Qinglong Road, Mianyang, Sichuan 621010, China

Supporting Information

ABSTRACT: Acid–base properties exert important influences on biochar's practical application as a soil amendment or contaminant sorbent. In this paper, a model with independent acidic/basic sites coexisting on a biochar surface is proposed to account for the acid–base behavior of biochar derived from two invasive species (*Spartina alterniflora* and water hyacinth). Modeling results show that a three-site model with two acidic sites and one basic site can reflect the acid–base behavior of biochar, increasing pyrolysis temperature results in the change in concentration (basic sites increase successively, while acidic sites decrease first and then increase) and strength (individual site dependent) of acidic and basic sites. Both the concentration and strength of the sites play important roles in the acid–base behavior of biochar. Theoretical simulations based on modeling results demonstrate that both surface net and local charge should be considered when electrostatic interaction is responsible for the biochar's environmental behavior. The site modeling procedure proposed in this study constructs a bridge between macroscopic pH and microscopic sites and is useful to describe the acid–base behavior of biomass and biomass-derived biochar.

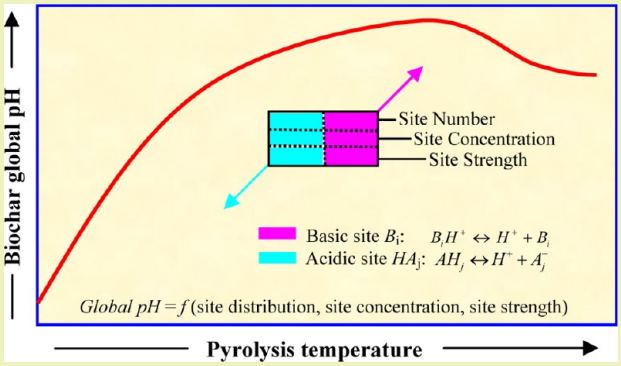

KEYWORDS: *Biochar, Acid–base behavior, Acidic/basic site, Mass titration, Potentiometric mass titration*

INTRODUCTION

Biochar, a form of black carbon (BC) generated from biomass thermochemical decomposition,[1] has received considerable interest in recent years due to its confirmed roles in soil amendment and carbon sequestration, as well as contaminant sorption.[2−5] Biochar can exhibit significant physicochemical differences due to diverse biomass feedstock and pyrolysis conditions, of which pyrolysis temperature is a key determinant.[6−8] Therefore, information regarding the transition in the structure and features of biochar generated under varying pyrolysis temperatures can provide significant insight into the selection and tailoring of biochar with properties beneficial for various purposes, for example, soil fertilization and contaminant sorption.

A recently proposed formation mechanism indicates biochar experiences dehydration, oxidation, and condensation/aromatization successively,[8] with structures evolving from heat-altered biopolymers over an amorphous mixture of heat-altered biopolymers and polyaromatic structures and finally toward graphite-like microcrystallite with increasing charring temperature.[7] It was revealed that physical and chemical properties of biochar, such as aromaticity,[6] hydrophobicity,[2] polarity,[7] recalcitrance index (R_{50}),[9] specific surface area,[6,7] surface pH,[2] and cation exchange capacity,[8] change monotonically with an increase in pyrolysis temperature or attain a maximum/minimum at a certain critical temperature. Gradual change in sorption behavior toward organic contaminants by biochar with pyrolysis temperature has been detected[4,6,10,11] in sorption isotherms (from linear to concave-downward), isotherm modeling (from dual absorption–adsorption model to exclusive adsorption model), and sorption mechanisms (from partition into noncarbonized organic medium to adsorption on carbonized phase), as well as sorption kinetics (from fast to low and then to fast). Regarding heavy metals immobilization, shifts in the sorption mechanism from cation exchange and complexation with oxygenated functional groups to chemical precipitation and cation–π bonding with electron-rich graphene-like aromatic structures were also reported.[12,13]

Acid–base properties exert a significant impact on the performance of biochar acting as a soil amendment or contaminant sorbent,[2,5,12,14−16] but only sparse information is available in theliterature elucidating the evolution of the acid–base character pertaining to pyrolysis temperature. Although macroscopic information on biochar acid–base properties, for example, surface pH and total acidity/basicity, has been reported by some researchers,[2,10,11] microscopic information,

Received: March 5, 2014
Revised: September 22, 2014
Published: October 6, 2014

such as the nature, abundance, and strength of acidic/basic sites, is also important but very limited in the literature. In this work, a model assuming independent acidic and basic sites coexisting on the surface is proposed to account for the acid–base behavior of biochar prepared over a wide temperature range. On the basis of the results from modeling, we pay further attention to the extent of surface ionization and the state of surface charging in given situations (e.g., a specific pH or sample mass concentration) and theoretically apply the principle of mass titration (MT)[17] and potentiomentric mass titration (PMT)[18] for pH_{pzc} determination of biomass and biomass-derived biochar.

EXPERIMENTAL SECTION

Preparation of Samples. Two invasive species, *Spartina alterniflora* (SA) and water hyacinth (WH, i.e., *Eichhornia crassipes*), were employed for biochar preparation. SA and WH were harvested from Chongming Island and Songjiang River, respectively, in Shanghai, China. The collected materials were tap water washed, sun dried, oven dried at 60 °C, and ground to pass through a 0.15 mm sieve to serve as raw biomass (SA 60, WH 60). The biochar sample was obtained by batch pyrolyzation of raw biomass under desired temperature (from 200 to 700 °C with increments of 100 °C) for 2 h and cooled to room temperature under nitrogen flow. More detailed information on the biochar production procedure is available in the Supporting Information. Pyrolysis products (referred as SA 200–700 and WH 200–700, number represents pyrolysis temperature) were crushed and sieved to less than 0.15 mm for further use. For removing soluble species, as suggested by Tsechansky and Graber,[19] all samples were washed with 0.05 M NaOH (20 g of sample per liter) by constant stirring for 24 h, rinsed with deionized water to a stable pH, dried at 80 °C for 48 h, and ground and sieved to less than 0.15 mm. Then, samples were further washed with 0.05 M HCl (12 g of sample per liter) with subsequent stirring, water rinsing, drying, grinding, and sieving similar to NaOH treatment. Both the original and base/acid-treated samples were employed for potentiometric titration.

Fourier transform infrared (FTIR) spectroscopy was employed to evaluate the surface functional group chemistry of the samples. The sample was mixed with KBr (potassium bromide) at a ratio of 1:100 (w/w) and pressed into a film. Infrared spectra were collected by a Thermo Scientific FTIR 380 spectrometer for wave numbers 400–4000 cm^{-1} at a scanning resolution of 4 cm^{-1}.

Potentiometric Titration. Fifty milliliters of 0.1 M NaCl as the background electrolyte was placed in a titration vessel, thermostated at 25 °C, stirred magnetically, and bubbled with humidified N_2 (40 mL min^{-1}) to eliminate atmospheric CO_2 interference. With the spurge of N_2, aqueous pH rose gradually, and a stable value of approximate 8 (hereafter referred to as pH*) was reached in 2 h. Then, samples (0.2 g) were introduced and equilibrated with an electrolyte solution for 24 h. After equilibrium, a stable pH was recorded as pH_{zpt} (the pH at the zero point of titration, that is, pH of suspension prior to addition of protons or hydroxyls).[20] If pH_{zpt} < pH*, the suspension was acidified with HCl to a pH of approximately 3; otherwise, NaOH was used to increase pH to approximate 11. After a new quasi-stable equilibrium was achieved (hereafter called the titration start point), titration was conducted by adding small increment of either HCl or NaOH. A stable pH (pH variation less than 0.01 per minute) at each addition of titrant was recorded for further model fitting. The experimental pH window of titration was limited to between 3 and 11 to avoid strong buffering from water outside this region.[21]

Titration data (pH as a function of titrant volume) were transformed in terms of charge balance in the titration system and reported as the change in sample surface charge (ΔQ) between titration point (Q) and titration start point (Q_0) according to eq 1. A detailed derivation procedure of eq 1 is given in the Supporting Information.

$$\Delta Q = Q - Q_0 = \frac{([H^+]_0 - [OH^-]_0) \times V_0 + N_t V - ([H^+] - [OH^-]) \times (V_0 + V)}{M} \quad (1)$$

where Q is the charge of sample surface at any point of titration (mmol g^{-1}). Q_0 is the sample charge corresponding to titration start point (mmol g^{-1}). $[H^+]_0$ and $[OH^-]_0$ are proton and hydroxyl concentrations in suspension at titration start point (mol L^{-1}), respectively. V_0 is the volume of suspension at titration start point (mL). N_t is the concentration of HCl or the negative value of NaOH concentration (mol L^{-1}). V is the cumulative addition volume of titrant (mL). $[H^+]$ and $[OH^-]$ are proton and hydroxyl concentrations at the titration point corresponding to titrant volume V (mol L^{-1}). M is the mass of sample (g).

Surface Ionization Model. The surface site can be amphoteric, acidic, or basic. Although the surface model with amphoteric sites and pure acidic sites is extensively employed in the literature,[22,23] a model with independent acidic and basic sites coexisting on the surface seems more realistic.[24−26] In this work, a nonelectrostatic discrete site model, based on a linear combination of completely independent acidic and basic sites, is assumed to characterize the complexity on thesample surface. Ionizations of the basic site, B_i, and acidic site, HA_j, are represented by the following chemical equilibria.

$$B_iH^+ \leftrightarrow H^+ + B_i,\ K_{B_iH^+} = \frac{[H^+][B_i]}{[B_iH^+]} \quad (2)$$

$$HA_j \leftrightarrow H^+ + A_j^-,\ K_{HA_j} = \frac{[H^+][A_j^-]}{[HA_j]} \quad (3)$$

Positive charges result from the protonation of basic sites, while negative charges are caused by the dissociation of acidic sites. The strength of the acidic site (HA_j) is described by its acidity constant (pK_{HAj}), and the strength of the basic site (B_i) is characterized by the constant of its conjugate acid ($pK_{B_iH^+}$).[27] Either the acidity or basicity constant fully describes the protolysis property of an acid–base pair. The stronger the acidity of an acid is, the weaker the basicity of its conjugate base is, and vice versa.[28]

In terms of mass action expressions (eqs 2 and 3) and mass balance, the surface net charge can be obtained from the sum of the local positive/negative charges

$$Q = \sum_i [B_iH^+] - \sum_j [A_j^-] = \sum_i \frac{b_i}{1 + \frac{K_{B_iH^+}}{[H^+]}} - \sum_j \frac{a_j}{1 + \frac{[H^+]}{K_{HA_j}}} \quad (4)$$

where b_i and a_j are the concentrations of the i^{th} basic site and the j^{th} acidic site (mmol g^{-1}), respectively. Notably, Q is high at the low edge of the pH window and low at the upper pH boundary.

By fitting ΔQ data to the postulated model based on eqs 1 and 4, the concentration (C) and equilibrium constant (pK_a) of an individual site, as well as Q_0, can be estimated. It should be noted that the resulting pK_a values are conditional or apparent rather than intrinsic because electrostatic effects were neglected in this model.

RESULTS AND DISCUSSION

pH_{zpt} of Samples. pH_{zpt} represents the pH of the sample suspension prior to titrant addition. The shift of biochar pH_{zpt} with respect to pyrolysis temperature provides global information on its acid–base behavior. The samples' pH_{zpt} values (original and base/acid treated) are compiled in Table S1 of the Supporting Informatin and are shown graphically in Figure 1. For the original samples, raw biomass is acidic (SA 60) or neutral (WH 60) in nature. Oxygen-free pyrolysis results in an increase in pH_{zpt}, that is, from pH 8.65 at 200 °C to 9.90 at 500 °C for SA and from 8.69 at 200 °C to 9.79 at 500 °C for

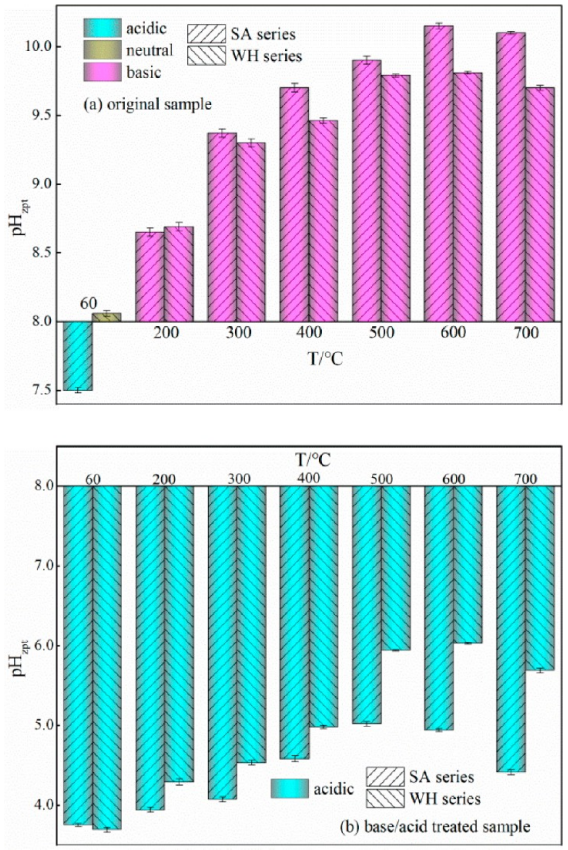

Figure 1. pH of sample suspension (pH_{zpt}) for original (a) and base/acid-treated (b) SA and WH series. Acid/base definition of samples is as follows: acidic when $pH_{zpt} < pH^*$, neutral when $pH_{zpt} \approx pH^*$, and basic when $pH_{zpt} > pH^*$.

WH. However, the maximal pH_{zpt} values for both the SA (10.15) and WH (9.81) series occurred at 600 °C rather than 700 °C. After the base/acid treatment, all samples become acidic with a pH_{zpt} shift with pyrolysis temperature in a manner similar to the original ones. The highest pH_{zpt} for both the original and base/acid-treated WH series occurred at 600 °C, while that for the original and base/acid-treated SA series occurred at 600 and 500 °C, respectively, indicating the significant influence of the soluble species on acid−base behavior. Even though a gradual upward trend in pH with pyrolysis temperature is common for biochar,[29−31] higher pH_{zpt} values achieved at the moderate instead of highest temperature have also been reported.[2,32,33] A possible explanation for this phenomenon is the decrease in concentration of Lewis base edge sites at higher temperature, which leads to low basicity and low pH.[34]

ΔQ(pH) of Samples. Both the original and base/acid-treated samples were employed for potentiometric titration. and the resultant titration data were transformed to ΔQ(pH) curves (Figure 2). It should be noted that ΔQ in eq 1 is a measure of the net excess charge upon a reference level (i.e., charge of the sample at the titration start point in this study). A positive ΔQ indicates charge excess, while a negative variation shows a charge deficiency relative to the reference level. From Figure 2, all ΔQ(pH) curves except SA 60 for the original samples (Figure 2 a, c) lie in positive region, while those from base/acid-treated samples (Figure 2 b, d) fall in a negative region over the entire pH domain examined. Diverse ΔQ(pH) curves related to pyrolysis temperature illustrate the existence of a varied acidity/basicity for both the original and base/acid-treated samples. The distinction between the ΔQ(pH) curves of the original and base/acid-treated samples suggests a significant impact of the soluble species and emphasizes the necessity to remove them before titration.[19] Therefore, only the ΔQ(pH) values of base/acid-treated samples were employed for subsequent modeling.

Modeling Procedure. For further insight into the biochar acid−base behavior, model fitting was carried out to quantitatively compare ΔQ(pH) and to estimate the detailed picture of the acidic/basic sites' distribution, abundance, and strength. In this process, we progressively increased the number of active sites and adjusted the partition of the acidic/basic sites to obtain the best result that can represent the simplest mathematical relation and provide an adequate description for the experimental phenomena. During ΔQ(pH) fitting, several acidic/basic site combinations produced equally good fits, which posed a great challenge for model selection. To choose appropriate acidic/basic site combinations, we assumed that these acidic/basic sites were placed in pure water (pH 7) and calculated equilibrium pH (pH_{cal}) according to the following charge balance equation

$$m\%\left(\sum_i \frac{b_i}{1+\frac{K_{B_iH^+}}{[H^+]}} - \sum_j \frac{a_j}{1+\frac{[H^+]}{K_{HA_j}}}\right) + [H^+] - [OH^-] = 0 \quad (5)$$

where m is the mass percentage of sample, for example, $m = 0.4$ in this experiment.

On the basis of the trend that pH_{zpt} changes with pyrolysis temperature and the principle that the deviation between pH_{cal} and 7.0 (pH for pure water) is close to that between pH_{zpt} and pH*, a set of combinations of acidic/basic sites were selected (Table S1, Supporting Information) and are shown graphically in Figure 3.

Analysis of Modeling Results. *Site Distribution.* Model fitting shows that generally a three-site model is good enough to describe the titration data for all base/acid-treated samples (Figure 2 b, d). When a three-site model is selected, there are four types of a partition model of acidic and basic sites: three-acidic-site model, two-acidic-site−one-basic-site model, one-acidic-site−two-basic-site model, and three-basic-site model. Modeling results show that the pH_{cal} values of a three-acidic-site model are too low and inconsistent with the experimental pH_{zpt} values. The pH_{cal} values of a one-acidic-site−two-basic-site model are essentially basic ($pH_{cal} > 7$), which is contradictory with acidic pH_{zpt} ($pH_{zpt} < pH^*$). The pH_{cal} values of a three-basic-site model are also basic and higher than that of a one-acidic-site−two-basic-site model. Only the pH_{cal} values of a two-acidic-site−one-basic-site model are relatively reasonable compared with the experimental pH_{zpt} values Thus, a two-acidic-site−one-basic-site model is selected for all samples (Figure 3). As shown, an alternative reason for the exclusion of the pure acidic or basic sites is the too low or high pH_{cal} values in terms of our modeling procedure.

Site Concentration. The concentration of the individual site, total acidic sites (T_a), and total basic sites (T_b) are shown in Figure 3 a and c. SA 60 and WH 60 have the highest T_a and lowest T_b compared to their pyrolysis products. With increasing pyrolysis temperature, T_b increases consecutively, while T_a decreases to a minimum at a critical temperature (500 °C in

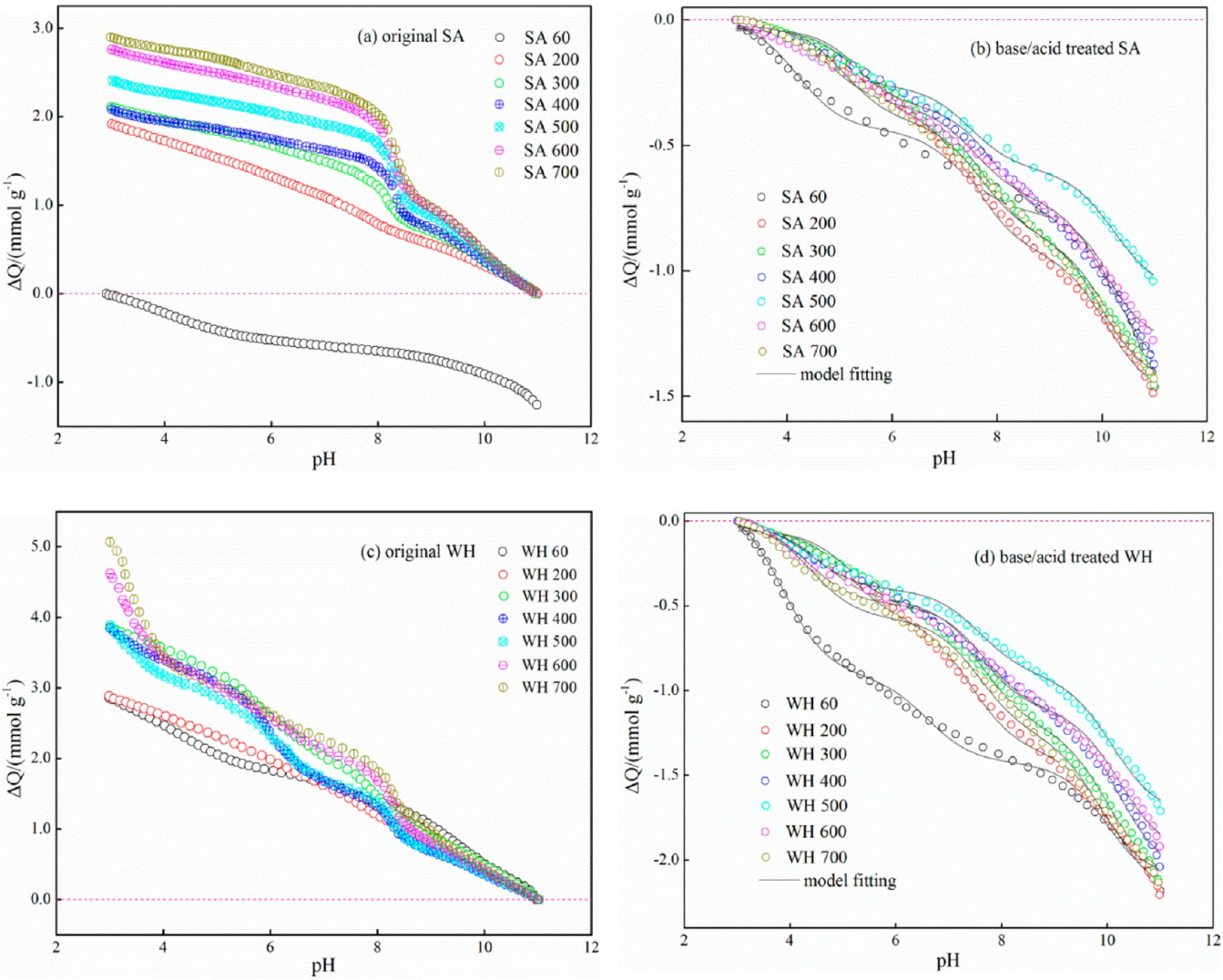

Figure 2. Experimental titration data reported as change in charge as a function of pH (ΔQ(pH)) transformed according to eq 1 in the text for original (a, c) and base/acid-treated (b, d) SA and WH series. Model fitting was carried out for base/acid-treated samples only.

this work) and then rises, which is consistent with experimental observation reported elsewhere.[10,33] Biochar surface acidity is usually caused by carboxyl groups (also in the form of their cyclic anhydrides), phosphonate, lactones or lactols, phenolic hydroxyl groups, and carbonyl groups (in the form of either isolated or arranged in quinone-like fashion).[23,35,36] Although most acidic sites would not withstand carbonization at high temperatures, some acidic sites might be formed as a result of oxygen chemisorption and subsequent oxidation in moisture air at room temperature,[37,38] which may account for the variation of T_a with pyrolysis temperature. Even though the origin of the surface basicity on the carbon materials is still under discussion, several basic sites are proposed, that is, oxygen-containing compounds (e.g., pyrones, chromenes), oxygen-free basic site ($C\pi$), nitrogen-containing groups (e.g., pyridines), superoxide ion (O_2^-), unsaturated valence, and inorganic matter.[25,39,40] In addition, the basicity on the carbon surface can also be ascribed to the redox reaction involving both pyrones[39] and delocalized electrons from the graphene sheet.[41] The increase in T_b can be attributed to both the elimination of acidity and the generation of basicity.[42] Examples include the foillowing: (1) The destruction of acidic groups decreases biochar acidity and therefore eliminates the neutralization effect of these sites to biochar basicity. (2) Thermal decomposition of oxygenated acidic groups forms active sites capable of fixing oxygen in the form of ether, which can rearrange with existing carbonyl groups to generate basic functional groups such as pyrones and chromenes. (3) The removal of oxygen from the carbon surface will delocalize free electrons associated with the basal planes of the carbon surface, allowing them to behave as Lewis base sites.

Site Strength. Besides site concentration, site strength is also an important contributor to acid−base reactivity. According to the definition mentioned above, the smaller the pK_a of an acidic site is, the stronger its acidity is, and the greater the pK_a of a basic site is, the stronger its basicity is. To homogenize the relationship between pK_a and acidity/basicity, we propose an index "strength factor (SF)" as follow: SF = −pK_a for an acid, and SF = pK_a for a base. Thus, the greater the SF is, the stronger the acidity/basicity is.

SF values of an individual site for each sample are shown in Figure 3 b and d. For both series, raw biomass exhibits three sites: a strong acidic site (SF = −4.20 for SA 60 and SF = −3.92 for WH 60), a weak acidic site (SF = −10.43 for SA 60 and SF = −9.97 for WH 60), and a moderate basic site (SF = 7.29 for SA 60 and SF = 6.66 for WH 60). Low and moderate temperature (200−400 °C) pyrolysis weakens both acidic and

dx.doi.org/10.1021/sc500432d | ACS Sustainable Chem. Eng. 2014, 2, 2501−2509

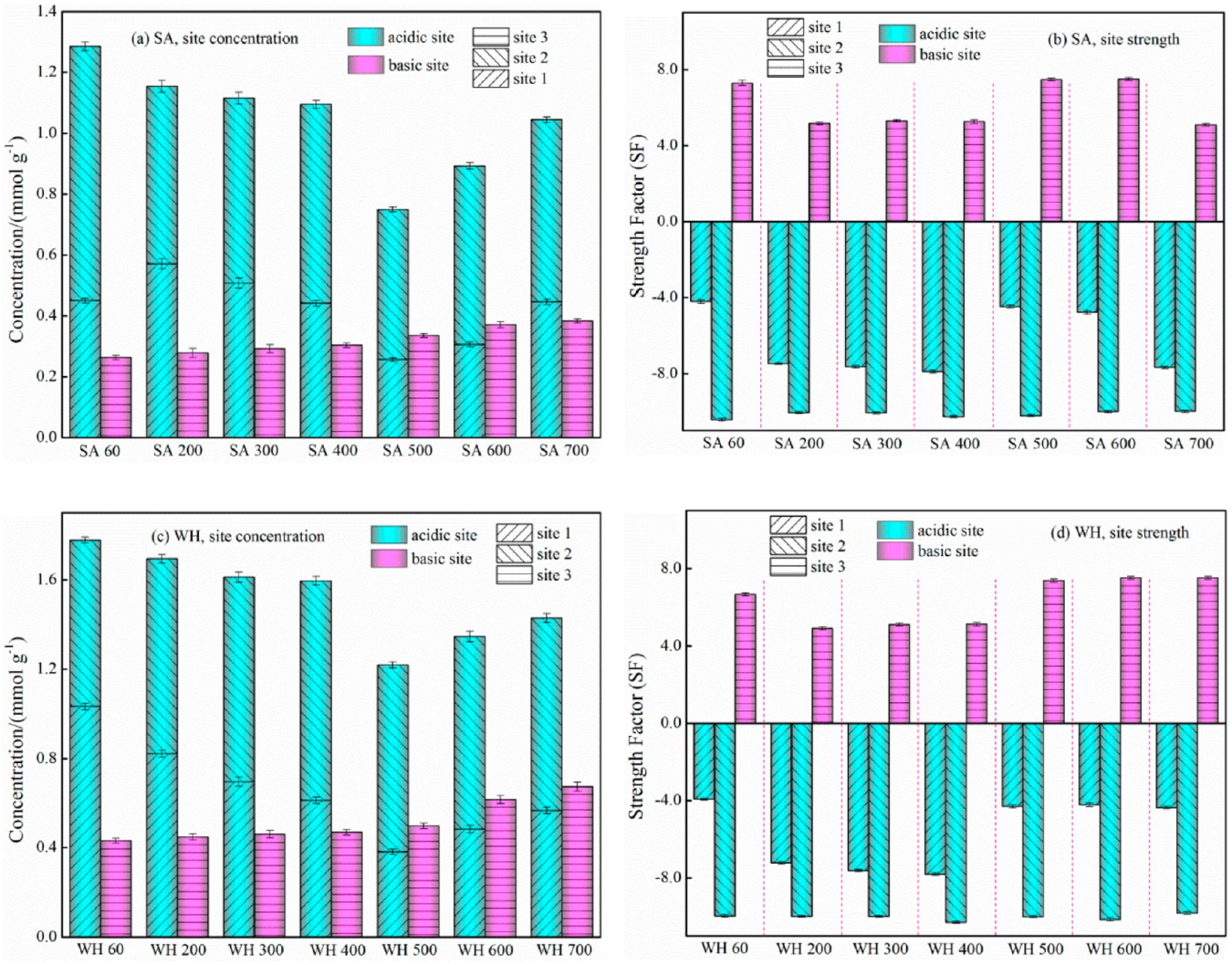

Figure 3. Site distribution, concentration, and strength factor (SF) for base/acid-treated SA (a) and WH (b) series. Strength factor (SF) is defined as follow: SF = $-pK_a$ for an acid and SF = pK_a for a base.

basic sites with more degrees for acidic sites. Further increasing the pyrolysis temperature (500−700 °C) leads to the enhancement in both acidic and basic sites except SA 700. The strength of acidic sites can be weak (SF < −9), moderate (−9 < SF < −5), or strong (SF > −5); however, the basic site is moderate or weak (SF < 9). The presence of strong basic sites (SF > 9) usually results in basic pH_{cal} (pH_{cal} > 7) in terms of our modeling results. In fact, approximately half of the combinations with two acidic sites and one basic site show basic pH_{cal} despite that T_a is much higher than T_b, indicating that the strength rather than the concentration of the basic site is more significant for determining acid−base reactivity.

Some acidic sites in the literature can be exemplified as carboxyl (pK_a = 1.7−4.7), phosphonate (pK_a = 6.1−6.8), lactones or lactols (pK_a = 6.37−10.25), and phenolic hydroxyls (pK_a = 9.5−13).[23,26,35] Basic sites receive less attention than acidic ones, and the nature and strength of them are still a point of debate. A possible origin of basic sites on carbon materials has been stated above, while the information about their pK_a values is very limited. Existing works have reported the presence of some basic sites with different strengths. For example, Contescu et al.[41] revealed a continuous basic pK_a distribution on a coconut-based carbon with three basic sites, a weak (pK_a 4−7), a moderate (pK_a 8.4−8.6), and probably a strong one (pK_a > 9.5). Similarly, by a continuous approach, Pagnanelli et al.[25] reported the existence of a basic site with pK_a = 5.2 on a carbonized olive pomace. In addition, a basic site corresponding to pK_a = 7.02 on a low-functionalized activated carbon was considered as arene centers (Cπ site).[43] On the other hand, a theoretical calculation suggested that pK_a of pyrones varied in a large interval (0−12).[39] The pK_a values of basic sites obtained in this manuscript fall in the range of the basic strength mentioned above and could deepen the understanding of the versatility of the strength of basic sites on biochar surfaces.

We cannot delineate unequivocal chemical identities to each site based on pK_a values alone because the structural diversity and complicated hierarchy of inter/intramolecular interactions usually make pK_a values vary in a wide range.[21,44] Therefore, FTIR was employed to identify the possible functional groups on the biochar. FTIR spectra (Figure S1, Supporting Information) reveal the existence of acidic sites as phenolic groups (1000−1200 cm^{-1}), quinones (1550−1680 cm^{-1}), carboxylic acids (1120−1200, 1665−1760, 2500−3300 cm^{-1}), and lactones (1160−1370, 1675−1790 cm^{-1}), and basic sites as

cyclic ethers (1025−1141 cm^{-1}) and pyrones (1450−1640 cm^{-1}).[7,45,46]

Charge at the Titration Start Point (Q_0). In the proposed model, Q_0 is the surface charge at the titration start point. A positive Q_0 is derived from protonated basic sites and a negative Q_0 from dissociated acidic sites. It should also be noted Q_0 includes the charges caused by strong acidic/basic sites, which can fully deprotonate or protonate within the experimental pH range. Therefore, it is only possible to estimate the amount rather than the strength of these sites from above model.

As shown in Table S1 of the Supporting Information, Q_0 of all samples is positive, and the shift with pyrolysis temperature is qualitatively in agreement with that of T_b. On the basis of the estimated concentration and strength of each site and eq 4, we calculated Q_0 (Q_0^{cal}) at pH 3 (Table S1, Supporting Information). Q_0^{cal} is generally lower than Q_0 acquired by $\Delta Q(pH)$ fitting, demonstrating that additional charge sources from sites with low pK_a (<3) are outside the experimental pH window.

Theoretical Simulation Based on Modeling Results. With the knowledge of (C, pK) pairs for surface sites, it is possible to predict how (C, pK) pairs influence surface charge as well as the extent of surface ionization. Moreover, we applied the principle of MT and PMT to theoretically verify the reliability of the proposed model.

Surface Net Charge. Surface net charges as a function of pH for the SA and WH series corresponding to 0.4% mass concentration are illustrated in Figure 4. The pH where net charge approaches zero is designated as theoretical point of zero charge pH_{tpzc} (Table S1). As shown, the variation of pH_{tpzc} with pyrolysis temperature is consistent with that of pH_{cal}.

A careful inspection of charge curves (Figure 4) shows that net charge (Q) increases with temperature at low pH values (e.g., pH 0−3) ,while first rises (60−500 °C) and then drops (500−700 °C) at high pH values (e.g., pH 11−14). At low pH values, net charge (positive) stems mainly from the protonation of basic sites, and thus, its change is in agreement with basic site concentration. At high pH values, on the other hand, net charge (negative) comes dominantly from the dissociation of acidic sites, and its change coincides with acidic site concentration. At intermediate pH values, net charge (positive, negative or null) is the competitive results of the acidic site's dissociation and basic site's protonation. Therefore, no obvious relationship between net charge and the concentration of active sites can be observed.

Figure 4 also shows that pH can greatly influence the net charge for a given sample, that is, the closer the pH approaches pH_{tpzc}, the smaller the net charge, and the further the pH is away from pH_{tpzc}, the greater the net charge. This information is helpful for understanding electrostatic interaction between biomass/biochar samples and charged species.

Surface Local Charge. In view of the model we adopted, the species that contribute to surface local charge are B_iH^+ and A_j^-. As indicated by eq 4, surface local charge depends on the concentration and pK_a of the acidic/basic site as well as environmental pH. Thus, different samples (i.e., with different concentrations and pK_a values of surface sites) may show different surface local charges. We take SA 400 and WH 500 as representatives to present the change of local charge with respect to pH (Figure 5), and the information on other samples is available in Figure S2 of the Supporting Information. For SA 400, when pH approaches pH_{tpzc}, not only is the net charge close to zero, but also the local charge is very low. In the case of

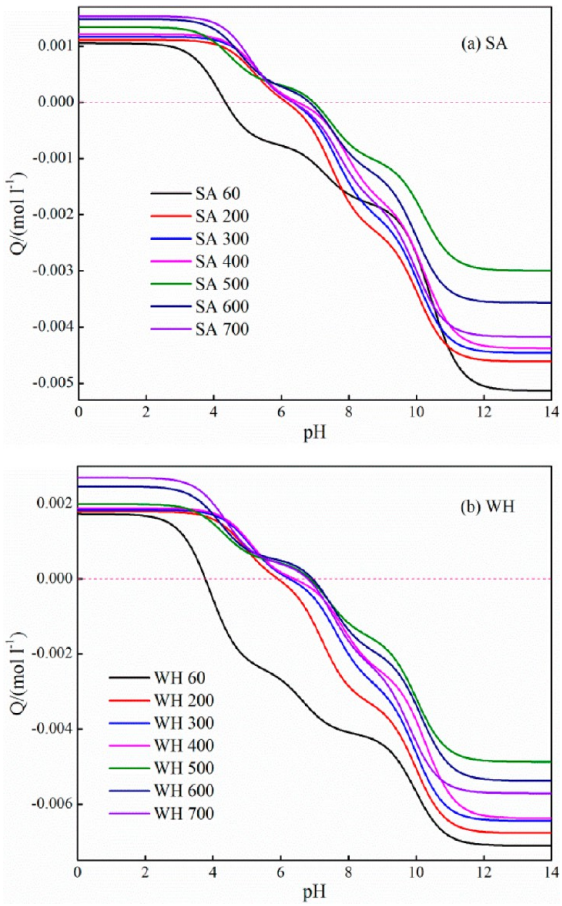

Figure 4. Variation in surface net charge as a function pH corresponding to 0.4% mass concentration for SA (a) and WH (b) series (base/acid treated).

WH 500, on the other hand, both local positive and negative charges are high even at pH_{tpzc}. The existence of a local charge even at pH_{tpzc} is necessary because it supplies hydrogen ions to establish the final equilibrium pH.[47] Consequently, besides net charge, local charge can provide additional insight into the interaction between samples and cations/anions caused by electrostatic attraction/repulsion.

Theoretical Application of MT and PMT. Solid pH is actually the pH of a solid suspension, which usually changes with its mass concentration. However, solid pH_{pzc} is intrinsic and thus independent of mass concentration. The classical MT method proposes that the limiting or asymptotic solid pH as a function of mass concentration is pH_{pzc}.[17] The later-developed PMT presumes that the pH corresponding to the common intersection point of potentiometric curves with different mass concentration is pH_{pzc}.[18] On the basis of MT and PMT principles and eq 5, we carried out theoretical pH calculations in terms of MT with a graphical proof following PMT for the determination of pH_{pzc} across a mass concentration range of 0.01−20%.[17,48]

Results (Table S2, Supporting Information) show that the calculated equilibrium pH_{cal} approaches pH_{tpzc} with an increase in mass concentration. In addition, it seems that MT is more sensitive when pH_{tpzc} is further away from neutrality. A previous model with one amphoteric site[17,48] or two independent acidic and basic sites[24] showed the validity of MT for pH_{pzc} determination. The model adopted here assuming several independent acidic/basic sites seems more

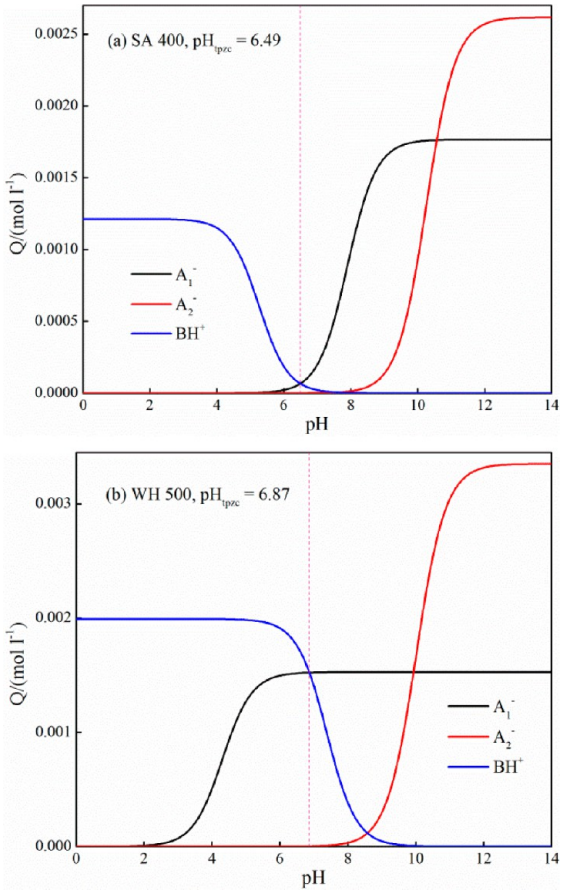

Figure 5. Variation in surface local charge as a function of pH corresponding to 0.4% mass concentration with SA 400 (a) and WH 500 (b) (base/acid treated) as representatives.

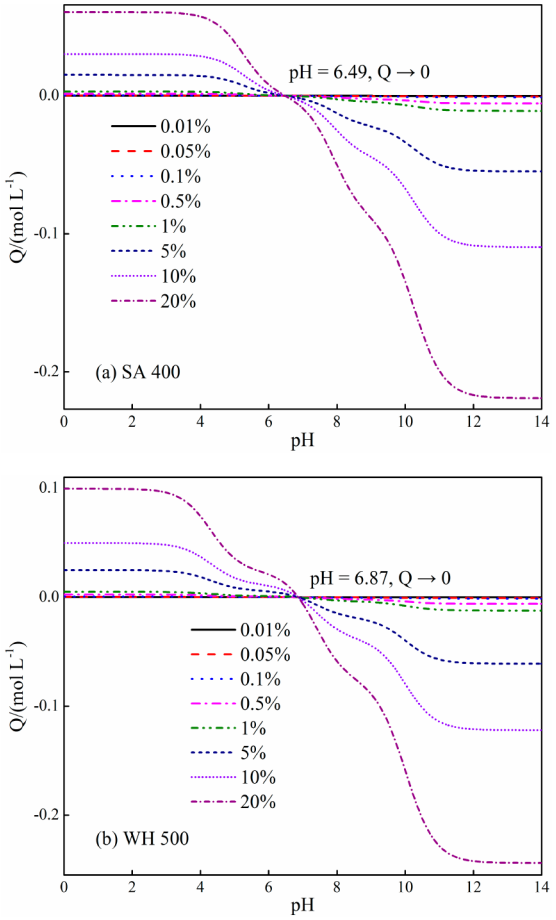

Figure 6. Variation in surface net charge as a function of mass concentration (0.01−20%) with SA 400 (a) and WH 500 (b) (base/acid treated) as representative.

practical for a heterogeneous solid surface and can be considered as an extension of MT validation. In accordance to Figure 5, surface net charges as a function of mass concentration for SA 400 and WH 500 are displayed in Figure 6, and other samples are shown in Figure S3 of the Supporting Information. As observed, net charge curves with different mass concentrations intersect at the same pH value, that is, pH_{tpzc}, which is consistent with PMT. Likewise, the net charge at the point of pH_{tzpc} is independent of mass concentration and is always zero; however, the net charge for other pH values increases with increasing mass concentration. Theoretical simulation of PMT demonstrated that pH_{pzc} does not depend on the surface ionization model and electrostatic model.[18] The results shown here indicate that PMT is also suitable for pH_{pzc} determination of biomass[49] and its charred counterparts, which is biochar.

Emphasis on pH_{zpt}, pH_{cal} and pH_{tpzc}. The relationship between pH_{zpt}, pH_{cal}, and pH_{tpzc} in this manuscript should be well understood. pH_{zpt} is an experimental pH of sample suspension and reflects the acid−base reactivity of the sample. pH_{cal} is the calculated equilibrium pH assuming that acidic/basic sites are immersed in pure water with the purpose of helping the model selection. pH_{tpzc} is the pH when the surface net charge approaches zero on the basis of modeling results and can be theoretically linked with pH_{cal} by the MT method. However, because of the difference between pH_{zpt} and pH_{cal}, theoretical pH_{tpzc} is not necessarily the actual pH_{pzc} of the samples. Although we cannot get perfect agreement between pH_{zpt} and pH_{cal} (and more efforts should be made to improve the surface model and modeling procedure), at least the consistency of their change with pyrolysis temperature can to some degree provide the basis for interpreting the acid−base behavior of biochar. Furthermore, the theoretical pH calculation of MT indicates that the pH_{zpt} of the concentrated suspension is perfectly adequate to represent pH_{pzc}.

Environmental Significance. Results from this study reveal that the degree of ionization of surface sites and the amount of surface net/local charge on biochar vary with environmental pH in a manner much too complex to be adequately described by a single isolated parameter pH_{pzc} or a condensed inventory based on a global classification scheme (Boehm method). For fully understanding biochar acidity/basicity, the knowledge of site concentration is not sufficient, and the acidic/basic constant of each site is also essential.

By using the approach established in this study, a full picture of the distribution, concentration, and strength of the individual acidic/basic sites on biochar surfaces can be depicted, and detailed acid−base behavior of the biochar can also be estimated. Briefly, the results from site modeling can be used to achieve following goals: (1) to predict surface net charge and local charge at a specified pH and solid concentration, (2) to predict the extent of surface ionization and the concentration of charged/uncharged species at a specified pH and solid concentration, (3) to predict equilibrium pH_{cal} for a specified solid concentration and theoretical pH_{tpzc}, and (4) to predict

dx.doi.org/10.1021/sc500432d | ACS Sustainable Chem. Eng. 2014, 2, 2501−2509

the amount of solid to be added into ambient media (such as water, soil) for achieving a desired pH. The former two are helpful to understand the interaction between biochar and charged species (e.g., heavy metal cations/anions and ionizable organic compounds),[2,14,15] and the latter two are meaningful for biochar's practical application acting as an environmental pH modifier.

This study indicates that pyrolysis temperature can affect both the concentration and strength of acidic/basic sites on biochar surfaces. Detailed information on individual acidic/basic sites can provide significant insight into the optimization of biochar production and guide its practical application for special purposes. For example, according to our results, if the alkalinity of biochar (from both inorganic matter and other origins of basicity as mentioned previously, with the former being more important) is desired,[38] pyrolysis would be performed at 600 °C because at this temperature the basicity of biochar is high (relative to lower temperatures) and stable (relative to higher temperatures).

The two species employed in this work, *Spartina alterniflora* and water hyacinth (*Eichhornia crassipes*), have invaded many countries (e.g., China and United States) of the world[50] and have led to severely social, economic, and ecological problems in local areas. Therefore, converting these invasive plants into valuable biochar can improve the invasive plant management and alleviate ecological and environmental concerns caused by them. As indicated by other researchers,[6−8] both biomass feedstock and pyrolysis conditions exert important influence on biochar's physicochemical properties. Therefore, one cannot expect that the information on the distribution, concentration, and strength of acidic/basic sites obtained from this study is generalized to other biomass types. However, we believe the approach proposed in this research is useful to describe acid−base behavior, and future investigations of various types of biomass and its derived biochar will help to refine the presented methodology.

■ ASSOCIATED CONTENT

Supporting Information

Information as mentioned in the text. This material is available free of charge via the Internet at http://pubs.acs.org.

■ AUTHOR INFORMATION

Corresponding Authors

*Phone: +86 21 66137743. Fax: +86 21 66137761. E-mail: qliu@shu.edu.cn (Q.L.).
*Phone: +86 21 66137758. Fax: +86 21 66137758. E-mail: grqian@shu.edu.cn (G.Q.).

Notes

The authors declare no competing financial interest.

■ ACKNOWLEDGMENTS

The authors are grateful for the financial supports from the Engineering Research Center of Biomass Materials (SWUST) (10zxbk05), Science and Technology Commission of Shanghai Municipality (12231204902), and Program for Innovative Research Team in University (IRT13078). We also greatly appreciate the thoughtful comments and constructive suggestions from anonymous reviewers for the improvement of this manuscript.

■ REFERENCES

(1) Preston, C. M.; Schmidt, M. W. I. Black (pyrogenic) carbon: A synthesis of current knowledge and uncertainties with special consideration of boreal regions. *Biogeosciences* **2006**, *3*, 397−420.
(2) Uchimiya, M.; Wartelle, L. H.; Klasson, K. T.; Fortier, C. A.; Lima, I. M. Influence of pyrolysis temperature on biochar property and function as a heavy metal sorbent in soil. *J. Agric. Food Chem.* **2011**, *59*, 2501−2510.
(3) Meyer, S.; Glaser, B.; Quicker, P. Technical, economical, and climate-related aspects of biochar production technologies: A literature review. *Environ. Sci. Technol.* **2011**, *45*, 9473−9483.
(4) Chen, Z.; Chen, B.; Chiou, C. T. Fast and slow rates of naphthalene sorption to biochars produced at different temperatures. *Environ. Sci. Technol.* **2012**, *46*, 11104−11111.
(5) Manyà, J. J. Pyrolysis for biochar purposes: A review to establish current knowledge gaps and research needs. *Environ. Sci. Technol.* **2012**, *46*, 7939−7954.
(6) Chen, B.; Zhou, D.; Zhu, L. Transitional adsorption and partition of nonpolar and polar aromatic contaminants by biochars of pine needles with different pyrolytic temperatures. *Environ. Sci. Technol.* **2008**, *42*, 5137−5143.
(7) Keiluweit, M.; Nico, P. S.; Johnson, M. G.; Kleber, M. Dynamic molecular structure of plant biomass-derived black carbon (biochar). *Environ. Sci. Technol.* **2010**, *44*, 1247−1253.
(8) Harvey, O. R.; Herbert, B. E.; Kuo, L. J.; Louchouarn, P. Generalized two-dimensional perturbation correlation infrared spectroscopy reveals mechanisms for the development of surface charge and recalcitrance in plant-derived biochars. *Environ. Sci. Technol.* **2012**, *46*, 10641−10650.
(9) Harvey, O. R.; Kuo, L. J.; Zimmerman, A. R.; Louchouarn, P.; Amonette, J. E.; Herbert, B. E. An index-based approach to assessing recalcitrance and soil carbon sequestration potential of engineered black carbons (biochars). *Environ. Sci. Technol.* **2012**, *46*, 1415−1421.
(10) Zhou, Z.; Shi, D.; Qiu, Y.; Sheng, D. Sorptive domains of pine chars as probed by benzene and nitrobenzene. *Environ. Pollut.* **2010**, *158*, 201−206.
(11) Chun, Y.; Sheng, G.; Chiou, C. T.; Xing, B. Compositions and sorptive properties of crop residue-derived chars. *Environ. Sci. Technol.* **2004**, *38*, 4649−4655.
(12) Uchimiya, M.; Lima, I. M.; Klasson, K. T.; Chang, S.; Wartelle, L. H.; Rodgers, J. E. Immobilization of heavy metal ions (Cu^{II}, Cd^{II}, Ni^{II}, Pb^{II}) by broiler litter-derived biochars in water and soil. *J. Agric. Food Chem.* **2010**, *58*, 5538−5544.
(13) Harvey, O. R.; Herbert, B. E.; Rhue, R. D.; Kuo, L. J. Metal interactions at the biochar−water interface: Energetics and structure−sorption relationships elucidated by flow adsorption microcalorimetry. *Environ. Sci. Technol.* **2011**, *45*, 5550−5556.
(14) Ni, J.; Pignatello, J. J.; Xing, B. Adsorption of aromatic carboxylate ions to black carbon (biochar) is accompanied by proton exchange with water. *Environ. Sci. Technol.* **2011**, *45*, 9240−9248.
(15) Teixidó, M.; Pignatello, J. J.; Beltrán, J. L.; Grenados, M.; Peccia, J. Speciation of the ionizable antibiotic sulfamethazine on black carbon (biochar). *Environ. Sci. Technol.* **2011**, *45*, 10020−10027.
(16) Abit, S. M.; Bolster, C. H.; Cai, P.; Walker, S. L. Influence of feedstock and pyrolysis temperature of biochar amendments on transport of *Escherichia coli* in saturated and unsaturated soil. *Environ. Sci. Technol.* **2012**, *46*, 8097−8105.
(17) Noh, J. S.; Schwarz, J. A. Estimation of the point of zero charge of simple oxides by mass titration. *J. Colloid Interface Sci.* **1989**, *130*, 157−164.
(18) Bourikas, K.; Vakros, J.; Kordulis, C.; Lycourghiotis, A. Potentiometric mass titrations: experimental and theoretical establishment of a new technique for determining the point of zero charge (pzc) of metal (hydr)oxides. *J. Phys. Chem. B* **2003**, *107*, 9441−9451.
(19) Tsechansky, L.; Graber, E. R. Methodological limitations to determining acidic groups at biochar surfaces via the Boehm titration. *Carbon* **2014**, *66*, 730−733.

(20) Silber, A.; Levkovitch, I.; Graber, E. R. pH-dependent mineral release and surface properties of cornstraw biochar: Agronomic implications. *Environ. Sci. Technol.* **2010**, *44*, 9318−9323.
(21) Contescu, A.; Contescu, C.; Putyera, K.; Schwarz, J. A. Surface acidity of carbons characterized by their continuous pK distribution and Boehm titration. *Carbon* **1997**, *35*, 83−94.
(22) Ali Ahmad, M.; Prelot, B.; Dufour, F.; Durupthy, O.; Razafitianamaharavo, A.; Marc Douillard, J.; Chaneac, C.; Villiéras, F.; Zajac, J. Influence of morphology and crystallinity on surface reactivity of nanosized anatase TiO2 studied by adsorption techniques. 2. solid-liquid interface. *J. Phys. Chem. C* **2013**, *117*, 4459−4469.
(23) Volesky, B. Biosorption and me. *Water Res.* **2007**, *41*, 4017−4029.
(24) Carrott, P. J. M.; Ribeiro Carrott, M. M. L.; Estevao Candeias, A. J.; Prates Ramalho, J. P. Numerical simulation of surface lonisation and specific adsorption on a two-site model of a carbon surface. *J. Chem. Soc., Faraday Trans.* **1995**, *91*, 2179−2184.
(25) Pagnanelli, F.; Mainelli, S.; Toro, L. New biosorbent materials for heavy metal removal: Product development guided by active site characterization. *Water Res.* **2008**, *42*, 2953−2962.
(26) Martín-Lara, M. A.; Blázquez, G.; Ronda, A.; Pérez, A.; Calero, M. Development and characterization of biosorbents to remove heavy metals from aqueous solutions by chemical treatment of olive stone. *Ind. Eng. Chem. Res.* **2013**, *52*, 10809−10819.
(27) Busca, G. Bases and basic materials in chemical and environmental processes. Liquid versus solid basicity. *Chem. Rev.* **2010**, *110*, 2217−2249.
(28) Stumm, W.; Morgan, J. J. *Aquatic Chemistry: Chemical Equilibria and Rates in Natural Waters*, 3rd, ed.; John Wiley & Sons: New York, 1996.
(29) Kim, P.; Johnson, A.; Edmunds, C. W.; Radosevich, M.; Vogt, F.; Rials, T. G.; Labbé, N. Surface functionality and carbon structures in lignocellulosic-derived biochars produced by fast pyrolysis. *Energy Fuels* **2011**, *25*, 4693−4703.
(30) Lehmann, J. Bio-energy in the black. *Front. Ecol. Environ.* **2007**, *5*, 381−387.
(31) Mukherjee, A.; Zimmerman, A. R.; Harris, W. Surface chemistry variations among a series of laboratory-produced biochars. *Geoderma* **2011**, *163*, 247−255.
(32) Bagreev, A.; Bandosz, T. J.; Locke, D. C. Pore structure and surface chemistry of adsorbents obtained by pyrolysis of sewage sludge-derived fertilizer. *Carbon* **2001**, *39*, 1971−1979.
(33) Uchimiya, M.; Chang, S.; Thomas Klasson, K. Screening biochars for heavy metal retention in soil: role of oxygen functional groups. *J. Hazard. Mater.* **2011**, *190*, 432−441.
(34) Menéndez, J. A.; Xia, B.; Phillips, J.; Radovic, L. R. On the modification and characterization of chemical surface properties of activated carbon: Microcalorimetric, electrochemical, and thermal desorption probes. *Langmuir* **1997**, *13*, 3414−3421.
(35) Boehm, H. P. Some aspects of the surface chemistry of carbon blacks and other carbons. *Carbon* **1994**, *32*, 759−769.
(36) Boehm, H. P. Surface oxides on carbon and their analysis: A critical assessment. *Carbon* **2002**, *40*, 145−149.
(37) Puziy, A. M.; Poddubnaya, O. I.; Martínez-Alonso, A.; Suárez-García, F.; Tascón, J. M. D. Synthetic carbons activated with phosphoric acid I. Surface chemistry and ion binding properties. *Carbon* **2002**, *40*, 1493−1505.
(38) Menéndez, J. A.; Phillips, J.; Xia, B.; Radovic, L. R. On the modification and characterization of chemical surface properties of activated carbon: In the search of carbons with stable basic properties. *Langmuir* **1996**, *12*, 4404−4410.
(39) Montes-Morán, M. A.; Suárez, D.; Menéndez, J. A.; Fuente, E. On the nature of basic sites on carbon surfaces: An overview. *Carbon* **2004**, *42*, 1219−1225.
(40) Drage, T. C.; Arenillas, A.; Smith, K. M.; Pevida, C.; Piippo, S.; Snape, C. E. Preparation of carbon dioxide adsorbents from the chemical activation of urea-formaldehyde and melamine-formaldehyde resins. *Fuel* **2007**, *86*, 22−31.
(41) Contescu, A.; Vass, M.; Contescu, C.; Putyera, K.; Schwarz, J. A. Acid buffering capacity of basic carbons revealed by their continuous pK distribution. *Carbon* **1998**, *36*, 247−258.
(42) Tessmer, C. H.; Vidic, R. D.; Uranowski, L. J. Impact of oxygen-containing surface functional groups on activated carbon adsorption of phenols. *Environ. Sci. Technol.* **1997**, *31*, 1872−1878.
(43) Arranz, P.; Bianchi, A.; Cuesta, R.; Giorgi, C.; Godino, M. L.; Gutiérrez, M. D.; López, R.; Santiago, A. Binding and removal of sulfate, phosphate, arsenate, tetrachloromercurate, and chromate in aqueous solution by means of an activated carbon functionalized with a pyrimidine-based anion receptor (HL). Crystal structures of $[H_3L(HgCl_4)]\cdot H_2O$ and $[H_3L(HgBr_4)]\cdot H_2O$ showing anion-π Interactions. *Inorg. Chem.* **2010**, *49*, 9321−9332.
(44) Kenney, J. P. L.; Fein, J. B. Cell wall reactivity of acidophilic and alkaliphilic bacteria determined by potentiometric titrations and Cd adsorption experiments. *Environ. Sci. Technol.* **2011**, *45*, 4446−4452.
(45) Fuente, E.; Menéndez, J. A.; Díez, M. A.; Suárez, D.; Montes-Morán, M. A. Infrared spectroscopy of carbon materials: A quantum chemical study of model compounds. *J. Phys. Chem. B* **2003**, *107*, 6350−6359.
(46) Stein, A.; Wang, Z. Y.; Fierke, M. A. Functionalization of porous carbon materials with designed pore architecture. *Adv. Mater.* **2009**, *21*, 265−293.
(47) Barton, S. S.; Evans, M. J. B.; Halliop, E.; Macdonald, J. A. F. Acidic and basic sites on the surface of porous carbon. *Carbon* **1997**, *35*, 1361−1366.
(48) Noh, J. S.; Schwarz, J. A. Effect of HNO_3 treatment on the surface acidity of activated carbons. *Carbon* **1990**, *28*, 675−682.
(49) Fiol, N.; Villaescusa, I. Determination of sorbent point zero charge: Usefulness in sorption studies. *Environ. Chem. Lett.* **2009**, *7*, 79−84.
(50) Global Invasive Species Database. Invasive Species Specialist Group (ISSG). http://issg.org/database/welcome/ (accessed October 2014).